THz Sensing Based on Subwavelength Metal Rectangular Grating in Attenuated Total Reflection Configuration

Vasily Valerievich Gerasimov[1, 2, a)], Oleg Eduardovich Kameshkov[1, 2], and Boris Alexandrovich Knyazev[1, 2]

[1]*Budker Institute of Nuclear Physics SB RAS, 11 Ac. Lavrentiev Ave., Novosibirsk 630090 Russia*
[2]*Laboratory of Applied Electrodynamics, Physics Department, Novosibirsk State University, 2 Pirogov St., Novosibirsk 630090 Russia*

[a)]*Corresponding author: v.v.gerasimov3@gmail.com*

Abstract. The sensing performance of a linear one-dimensional gold rectangular subwavelength grating platform with the ATR (Otto) coupling technique for gas detection has been numerically studied in the THz range. The optimal parameters of gratings for exciting surface plasmon resonances with a maximal efficiency were found. The dispersion analysis of surface waves confirmed the correctness of the reflection spectrum simulations. The fundamental and 1[st] order modes of deep grooves demonstrated a very high sensitivity to a small refractive index change up to 1.5 THz/RIU (in the frequency domain) and 557 deg/RIU (in the angular domain), with the refractive index detection limit of the sensor $7 \cdot 10^{-3}$ RIU and $1.5 \cdot 10^{-7}$ RIU, respectively. Compared with the fundamental modes, the high-order modes revealed the higher *FOM* values up to 500 1/RIU due to the narrow width of the resonances. These sensing characteristics are very promising for creating THz sensors based on subwavelength grating platforms.

INTRODUCTION

The terahertz (THz) spectral range is located between the microwave and infrared regions and covers frequencies from 0.1 to 10 THz (from 30 µm to 3 mm in wavelengths). As the THz photons have the quantum energy up to 40 meV, this radiation is nonionizing and many rotational and vibrational modes of complex intra- and extra-molecule bonds of biological substances in solid, liquid and gas form lie in the THz frequency range [1-2]. That is why the THz radiation is of great importance for biological, medical, industrial and security sensing applications [3-4].

One approach to achieve the strong light–matter interactions and sharp spectral features to enable the detection of small changes in the dielectric environment is using a method giving a strongly confined electromagnetic field, like surface plasmon polariton (SPP) sensing in visible range [5]. However, due to the high conductivity of metals in the THz range only poorly confined Sommerfeld-Zenneck waves can propagate along the smooth metal-dielectric interface with decay lengths in to the air of several centimeters ($100-1000\lambda$) [6]. To overcome this limitation Pendry *at el.* proposed the use of structured metal surfaces with holes in them to mimic the SPPs at much lower frequencies than the visible range [7]. These surface waves (called spoof surface plasmon polaritons (SSPP)) are bound TM electromagnetic surface modes having a high field coupling with the metamaterial structure even in the case of perfect electrical conductor (PEC) material [8]. The most frequently used label-free SSPP sensing platforms consist of subwavelength metal gratings [9-10] or waveguides including thin dielectric films [11].

In this paper, we focused on the SSPP sensing platform based on the one-dimensional subwavelength metal grating with attenuated total reflection (ATR) coupling technique (Otto configuration) [9, 12-13]. The common principle of operation of the sensor is an occurrence of a surface plasmon resonance (SPR) shift in the reflection spectrum, as a result of a change in the refractive index of the dielectric environment near the grating. Ng *at el.* were first experimentally demonstrated refractive index sensing of nitrogen and various fluids by monitoring sharp changes of SPRs in both amplitude and phase of the THz radiation using time-domain spectroscopy (TDS) technique [9]. The sensing performance can be assessed by common characteristics: the sensitivity (S = frequency shift / change of the analite refractive index) and figure of merit ($FOM = S / FWHM$), where $FWHM$ is a full width of the resonance dip at a half minimum. In [9], for nitrogen as an analite substance the sensitivity was attained $S \approx 0.49$ THz/RIU, $FOM \approx 49$ RIU^{-1}, and the refractive index detection resolution was $\Delta n = 0.02$ RIU. Yao and Zhong found the optimal configurations for a rectangular deep subwavelength metal grating and the optimal gap between the prism and grating producing both the fundamental and high-order modes of SSPP, at that high order modes had a higher sensitivity of up to 2.27 THz/RIU and $FOM \approx 262$ RIU^{-1} with $\Delta n = 0.004$ RIU [14]. Zhang and Han numerically investigated the angular spoof plasmon resonance vs. the change of the refractive index at 1 THz frequency [12]. For silicon prism and gold rectangular grating they attained an extremely high angular sensitivity ($S = 320°$/RIU) corresponding to the refractive index resolution $\Delta n = 3\cdot10^{-7}$ RIU (assuming 10^{-4} degree for angular resolution typically used in the optical SPR sensors), which is comparable with the performance of similar surface plasmon resonance sensors in visible range [5]. The analysis of the groove shapes (rectangle, triangle, trapezoid and slanted) in a 1D subwavelength gratings was shown, that trapezoid and slanted geometries gave the maximum sensor sensitivities [12, 15]. Huang *at el.* experimentally demonstrated that the metallic gratings could serve as perfect THz absorbers in an ATR geometry tunable in the wide range due to very strong SPRs [13].

Besides the subwavelength metal gratings, alternative more simple and law cast sensing platforms using diffraction metal gratings [16] and hybrid waveguide with a subwavelength plastic ribbon [17] were proposed in the THz region, giving the sensor sensitivities up to 0.5 THz/RIU and 0.26 THz/RIU, respectively.

In the current work, a sensing platform based on a linear one-dimensional metal rectangular grating using the ATR coupling technique was studied in the THz range by the numerical simulations. Using the model of effective medium and finite element method the performance of three configurations of SPR sensors was analyzed in the frequency and angular domain, and the optimal parameters allowing the maximal sensitivity were seek.

THEORY

The schema of the surface plasmon resonance exciting with the ATR technique in Otto configuration are presented in Fig. 1. The THz beam in the half-cylindrical prism incident on the interface between the prism (with refractive index n_p) and dielectric (with refractive index n_d) at the incident angle $\theta_{int} > \theta_{cr} = \arcsin\left(n_d / n_p\right)$, producing evanescent wave interacting with the subwavelength metal grating. In case of matching between the projection of k_p-vector of the incident wave in the prism on to x-axis and the spoof surface plasmon k-vector propagating along the grating, the evanescent wave was coupled into the SSPP

$$k_x = k_p \sin\left(\theta_{int}\right) = \frac{2\pi}{\lambda} n_p \sin\left(\theta_{int}\right) = k_{SSPP}\,, \tag{1}$$

where λ is the wavelength in vacuum. A one-dimensional grating having the period p, groove width w and depth d, in the limit of $p, w << \lambda$ can be modelled by the dielectric layer with the effective dielectric permittivity and plasma frequency, depending on the grating parameters [18, 7].

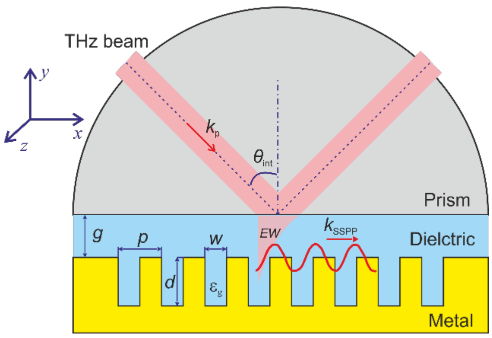

FIGURE 1. ATR Otto configuration for coupling of the SSPPs on the metal grating.

Taking the loss in metal into consideration, the SSPP k-vector can be expressed as [19]

$$k_{\mathrm{SSPP}} = \left(\varepsilon_{\mathrm{d}} k_0^2 + \left(\frac{w\varepsilon_{\mathrm{d}}}{p\varepsilon_g} \right)^2 k_g^2 \tan^2\left(k_g d\right) \right)^{1/2}, \tag{2}$$

where

$$k_g = k_0 \sqrt{\varepsilon_g} \left(1 + \frac{l_s\left(i+1\right)}{w} \right)^{1/2} \tag{3}$$

is a wave vector in groove; ε_{d}, ε_{g} – dielectric permittivities of substances in the gap and groove; $k_0 = 2\pi/\lambda$; $l_s = \left(k_0 \operatorname{Re}\sqrt{-\varepsilon_{\mathrm{m}}}\right)^{-1}$ is the skin depth of the metal with the dielectric permittivity ε_{m}.

Eq. 2 is the dispersion relation for SSPP propagating along the subwavelength grating, allowing the flexibility of designing of gratings for sensing applications. k_{SSPP} significantly depends on the groove depth d [19]. The wave vector of a surface wave propagating along the corrugated surface is limited by the first Brillioun zone, $k_0 < \pi/p$. Thus, according to Eqs. (2), (3), when $d < p\big/\sqrt{\varepsilon_{\mathrm{g}}}$, only fundamental mode (m=0) can be excited, while $d > mp\big/\sqrt{\varepsilon_{\mathrm{g}}}$ (m is an order of the mode), high order modes (up to m) can be supported by the grating [20]. Besides, as the grooves are opened, small amount of the high order mode electromagnetic field will extend into the dielectric and the "extending" electric field from adjacent grooves couple with each other and finally form the propagating wave [14]. According to the dispersion relation (2), the cutoff frequencies f_{c} can be found from the condition $k_{\mathrm{g}} d = \frac{\pi}{2}\left(m+1\right)$, which gives

$$f_{\mathrm{c}}^{\mathrm{m}} = \frac{c}{4d\sqrt{\varepsilon_{\mathrm{g}}}}\left(2m+1\right). \tag{4}$$

REFLECTION SPECTRA SIMULATIONS

We examined the simple sensing schema shown in Fig. 1. The grooves and gap between the grating and prism are filled with a gas having the refractive index n_{d} ("Gas detector").

The reflection coefficients in ATR configuration are measured vs. frequency or angle. In case of a wave vector matching condition according to Eq. (1), a surface plasmon resonance (SPR) will occur, producing the resonance dip in the reflection spectrum. A resonance frequency and reflection coefficient value depend on the grating parameters, gap and dielectric properties of substances in the grooves and gap.

Numerical simulations of reflection spectra were made using Comsol Multiphysics software by the finite element method (FEM). The simulation schema is shown in Fig. 2 (a). The regime of Floquet ports, unit cell and periodic left and right side boundary conditions (PBC) were employed. Floquet ports were also periodic and excited TM plane waves $\left(0,0,H_z\right)$ at an incident angle θ_{int}.

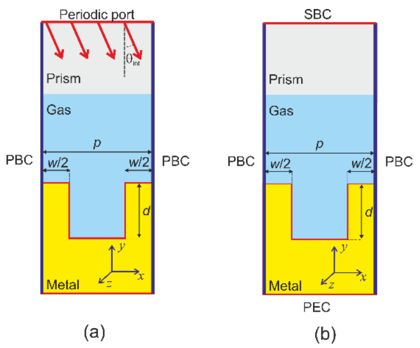

FIGURE 2. Simulations schemes for "Gas detector": (a) reflection spectrum; (b) dispersion analyses.

The choice of grating parameters is determined by the sample fabrication technique and working frequency range of available radiation sources. In our case we focused on the Novosibirsk free electron laser (NovoFEL) generated powerful monochromatic pulsed radiation at a repetition rate of 5.6 MHz in the frequency range of 1.5 – 3 THz (100 – 200 μm in the wavelength) [21]. In the below frequency region (0.2 – 2.5 THz), the available for us time-domain spectrometer [22] can be used. According to the restriction imposed on non-radiative waveguide modes by the first Brillioun zone [14], the period for subwavelength grating must be less than a half wavelength ($p < \lambda/2$), which correspond to $p < 50$ μm. We chose the period $p = 40$ μm and width $w = 20$ μm. For grooves with $d < 40$ μm (when air is in the grooves, $\varepsilon_g = 1$) only fundamental modes can be excited (see Theory Sec.), for $d > 40$ μm - fundamental and high-order modes. Such small width and deep grooves can't be made using the conventional UV photolithography with the acceptable quality. The multibeam X-ray lithography [23] or conventional deep reactive ion etching techniques [24] allow to obtain deep regular structures with the vertical walls with an accuracy no worse than 1 μm.

As a prism we used a high-resistive silicon having the refractive index $n_p = 3.42$ in THz region. The metal was gold with the Drude permittivity ($\omega_p = 1.38 \cdot 10^{16} c^{-1}$, $\omega_\tau = 4.05 \cdot 10^{13} c^{-1}$ [25]).

To find the optimal parameters of gratings we varied d (1 – 100 μm) and g (1-150 μm) depending on the refractive index of substances in the grooves and gap. The parameters were selected by the fallowing criteria: (1) minimum value of the reflection coefficient (less than 0.6) corresponding to a plasmon resonance; (2) stability of a resonance frequency when a slight variation of g (only a magnitude of the reflection coefficient changes); (3) gradual shifting of a resonance frequency when varying the refractive index in the grooves. In order to optimize the process of searching for optimal parameters, a special program in Matlab was written that managed the simulations in Comsol. It allowed to automate the large data processing.

The selected parameters obtained for "Gas detector", when the grooves and gap are filled with air ($n_g = n_d = 1$), are shown in Fig. 3. Each point correspond to the stable plasmon resonances at the incident angle $\theta_{int} = 45^o$ with the reflection coefficient $R \le 0.6$ and appropriate d, resonance frequency f_{res} and g. Shallow ($d < 40$ μm) fundamental and high order ($d > 40$ μm) modes lie in the frequency region generated by the NovoFEL, deep fundamental modes – in the TDS range. Points marked by red correspond to the deepest resonances. For such points we simulated the reflection spectra varying the refractive index in grooves. The results for the shallow grating ($d = 5$ μm, $g = 6$ μm) are presented in Fig. 4 (a). With increasing the refractive index n_d by the step $\Delta n = 0.01$, the resonance gradually shifts to the lower frequencies. By the linear fitting of the dependence f_{res} vs. n_d (see the red line in the inset B in Fig. 4 (b)), we got $f_{res} = 2.77 - 0.2 \cdot n_d$. This equation offers the sensitivity $S = \Delta f_{res}/\Delta n = 0.2$ THz/RIU, where Δf_{res} (THz) is a resonance shift arises from variation of n_d by step Δn.

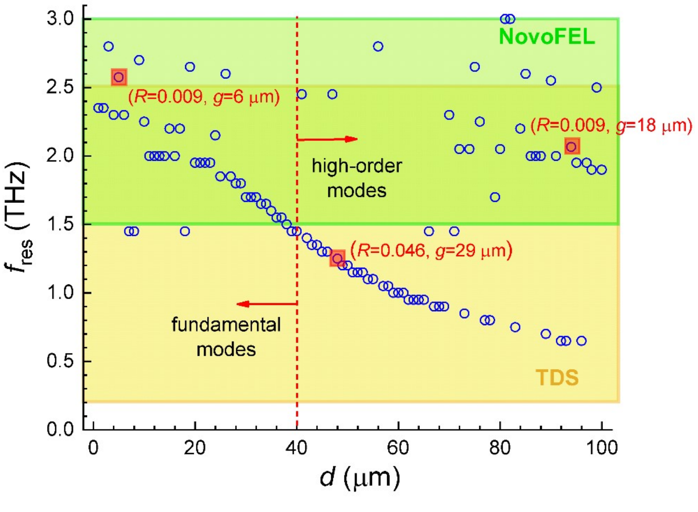

FIGURE 3. Resonance frequency vs. groove depth, obtained for "Gas detector" filled with air ($n_g = n_d = 1$) after the optimization: all points correspond to the stable plasmon resonances with $R \le 0.6$, points marked by red – minimum of R. Green

aria (1.5 – 3 THz) is a frequency region generated by the NovoFEL, beige aria (0.2 – 2.5 THz) – by a conventional TDS system. For $d < 40$ μm only fundamental modes can be excited, for $d > 40$ μm - fundamental and high order modes. The incident angle $\theta_{\text{int}} = 45^{\circ}$.

In sensing applications, the full width at the half minimum ($FWHM_f$) in the units of frequency (THz) is another important characteristic related with the quality factor (Q) of the resonance. It is clear that to minimize the overlapping between the detection thresholds upon shifting the resonance, resonances with a narrower bandwidth can be distinguished better in the experiment. For all resonances in Fig. 4(a) $FWHM_f \approx 0.004$ THz which correspond to the figure of merit $FOM = S/FWHM = 50$ RIU^{-1}.

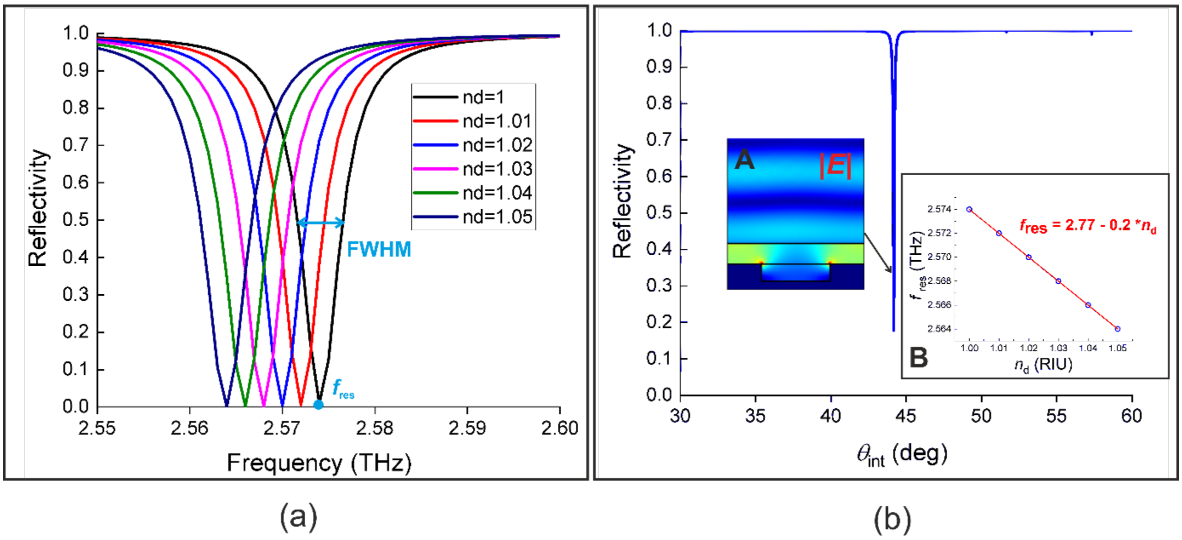

FIGURE 4. Reflection spectra for “Gas detector” ($n_g = n_d$) with $d = 5$ μm and $g = 6$ μm: (a) in the frequency domain at $\theta_{\text{int}} = 45^{\circ}$ for n_d variations with the step $\Delta n = 0.01$; (b) in the angular domain at the resonance $f_{\text{res}} = 2.57$ THz ($n_d = 1$). The inset A – $|E|$-field distribution near the groove, the inset B – dependence f_{res} vs. n.

When using a monochromatic radiation as the NovoFEL, in experiments a reflection spectrum can be measured in the angular domain. We simulated the angular spectrum for the shallow grating at the resonance frequency $f_{\text{res}} = 2.57$ THz ($n_d = 1$) (Fig. 4 (b)). There is a very narrow resonance at $\theta_{\text{int}} \approx 45^{\circ}$ with the bandwidth $FWHM_a \approx 5$ min ($Q \approx 530$). The resonance angle θ_{int} is slightly less than 45° due to uncertainties of the simulations. The field distribution $|E|$ at the resonance (see the inset A in Fig. 4 (b)) corresponds to fundamental mode, the most part of energy is concentrated under the groove.

The same numerical simulations were made for gratings with deeper grooves $d = 48$, 94 μm (Figs. 5-6). The sensing parameters for all gratings are summarized in Table 1. The sensitivities of deep gratings are much higher ($S = 1$-1.5 THz/RIU) due to the $|E|$-field distributions are more confined and concentrated in the grooves (insets B in Figs. 5-6). Despite the highest sensitivity for the grating with $d = 48$ μm, their resonance bandwidth is about two times larger compared with the shallow grating ($d = 5$ μm), which correspond to the higher Joule losses in the metal walls. The most narrow resonance is for $d = 94$ μm, giving the maximal FOM value (500 1/RIU). It can be explained by the high-order nature of the deep resonance (see the inset B in Fig. 6). In the experiments the $FWHM$ must be larger and FOM values – lower due to increase in absorption losses caused by the formation of hot spots at the structural imperfections in the real gratings and diffraction effects resulting from the scattering of the SSPPs modes at the edges of the grating [14].

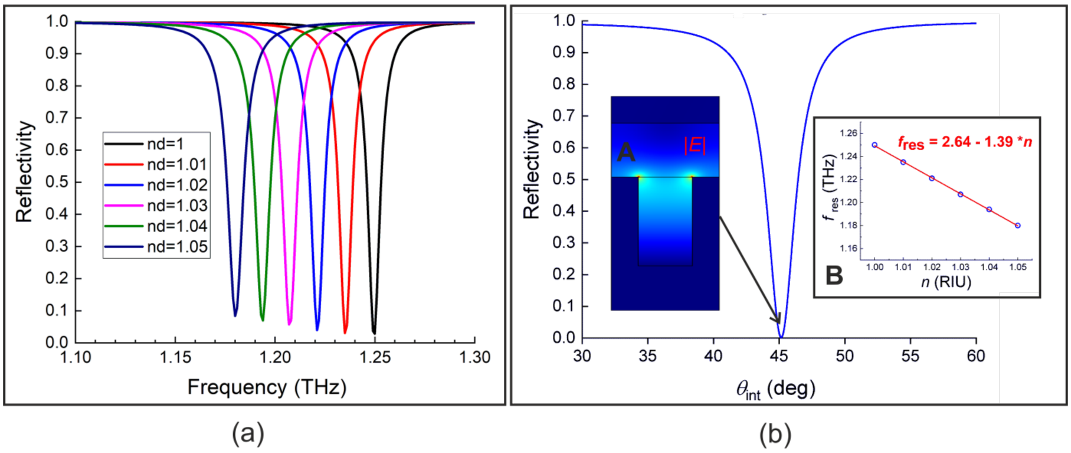

FIGURE 5. Reflection spectra for "Gas detector" ($n_g = n_d$) with $d = 48$ μm and $g = 29$ μm: (a) in the frequency domain at $\theta_{int} = 45°$ for n_d variations with the step $\Delta n = 0.01$; (b) in the angular domain at the resonance $f_{res} = 1.25$THz ($n_d = 1$). The inset A – |E|-field distribution near the groove, the inset B – dependence f_{res} vs. n.

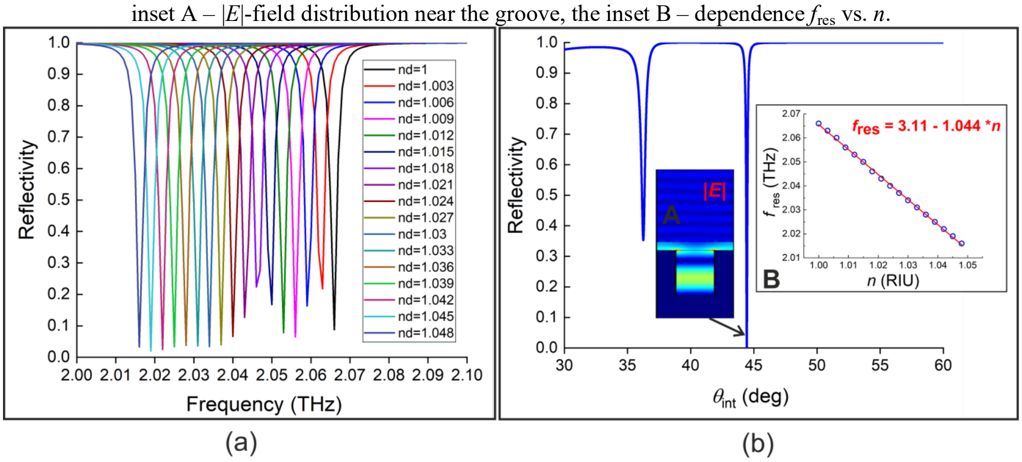

FIGURE 6. Reflection spectra for "Gas detector" ($n_g = n_d$) with $d = 94$ μm and $g = 18$ μm: (a) in the frequency domain at $\theta_{int} = 45°$ for n_d variations with the step $\Delta n = 0.003$; (b) in the angular domain at the resonance $f_{res} = 2.066$THz ($n_d = 1$). The inset A – |E|-field distribution near the groove, the inset B – dependence f_{res} vs. n.

TABLE 1. Sensing characteristics of gratings with optimal parameters.

Grating parameters	S (THz/RIU)	FWHM$_f$ (GHz)	FWHM$_a$ (min)	FOM (1/RIU)	δn_d (RIU)
$d = 5$ μm, $g = 6$ μm	0.2	4	5	50	0.05
$d = 48$ μm, $g = 29$ μm	1.5	7-10	155	140-214	0.007
$d = 94$ μm, $g = 18$ μm	1	2	6	500	0.01

The detection limit of the sensor is defined as

$$\delta n_d = \delta f_{res} / S, \tag{5}$$

where δf_{res} is a frequency resolution of a detector. In conventional TDS systems $\delta f_{res} = 10$GHz. The values for δn_d obtained by Eq. (5) are in the last column of Table 1. For the deep gratings, the detection limit is about five times better then for shallow grating. The sensing parameters, obtained for the deep grating with the high-order mode resonance at ≈ 2 THz, are comparable with the best results for high-order modes found in the literature [14].

To verify the sensing performance of our gratings in the angular domain more detail, we simulated the angular spectrum for the deep grating with $d = 48$ μm and $g = 29$ μm at the resonance frequency $f_{res} = 1.25$THz (see Fig. 7 (a)). With increasing incident angle the resonance angle gradually shifts towards higher angles, due to increasing the k_{SSPP}-vector. Using linear fitting of the dependence θ_{res} vs. n, the angular detection limit can be estimated by Eq. (5) replacing δf_{res} by $\delta\theta_{res} = 10^{-4}$ deg. If we use $\delta\theta_{res} = 10^{-4}$ deg, which is typically used in the optical SPR sensors [26], one can get the extremely high refractive index resolution up to $\delta n_d = 1.5 \cdot 10^{-7}$ RIU. It is possible due to a high angular sensitivity, which rises vs. the refractive index shift (Fig. 7 (c)) reaching up to 557 deg/RIU. These sensing parameters are better than ones reported in literature [12]. Due to the large *FWHM* values of angular resonances (Fig. 7 (d)), the *FOM* values are not high (Fig. 7 (e)). If we take deep high-order modes having high *Q*, the *FOM* parameter could be significantly increased.

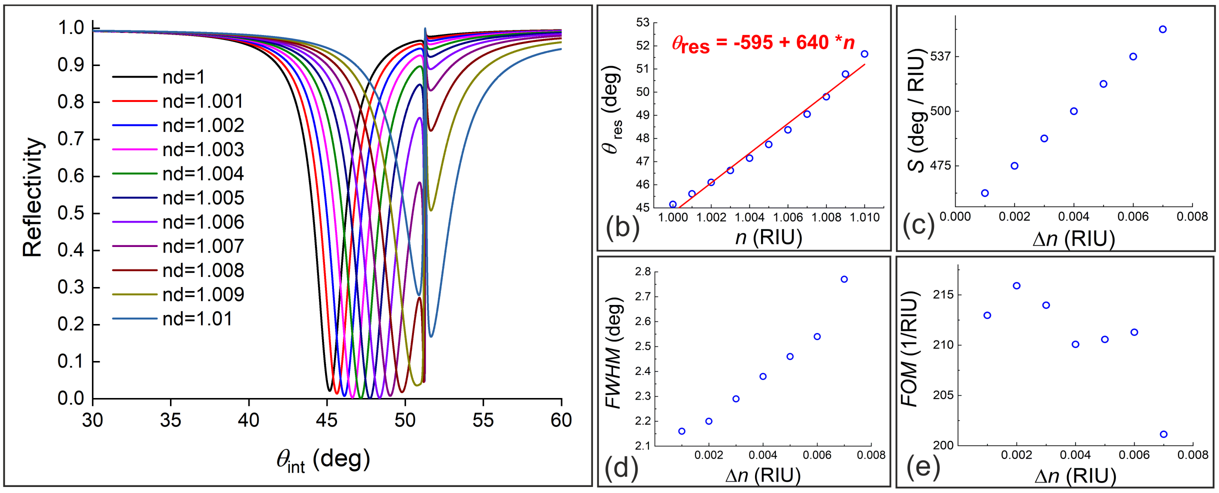

FIGURE 7. (a) Reflection spectra for “Gas detector” ($n_g = n_d$) with d = 48 μm and g = 29 μm at the resonance $f_{res} = 1.25$ THz (n_d = 1) in the angular domain for n_d variations with the step Δn = 0.001; (b) resonance angle θ_{res} vs. n; (c) sensitivity S vs. the refractive index shift Δn; (d) *FWHM* vs. Δn; (e) FOM vs. Δn.

DISPERSION ANALYSES

The additional method for study of SPRs is the dispersion analyses of surface modes. Results of this analysis are independent from the gap between the coupling prism and grating, allowing to verify the resonances in reflection spectra simulated in Comsol. We calculated dispersion curves of SSPPs by the effective medium model (Eq. 2) and finite element method (FEM). The FEM simulations were made in Comsol with the special solver of eigenmodes, without of using external sources and matching methods. The regime of Floquet ports and periodic left and right side boundary conditions applied to the structure’s unit cell were employed (see Fig. 2 (b)). The upper bound of the unit cell was modelled with scattering boundary conditions (SBC), the bottom bound – with perfect electric conductor (PEC). The optical parameters of the prism, metal and incident conditions were the same as in the reflection coefficient simulations. The wave vector was varied in the range of the first Brillouin zone.

Dispersion curves of SSPPs obtained for deep gratings with d = 48 μm and d = 94 μm are shown in Fig. 8. The lines of k_{SSPP} calculated from Eq. 2 are higher then lines simulated in Comsol. In can be caused by the following reasons: (1) the propagating SSPP is not the theoretical surface wave (as in the effective medium theory) when the gap is small; as a result, a considerable part of the energy will reradiate back into the prism [27]; (2) the destructive interference effect between the electromagnetic wave reflected at the prism-air interface and that reemitted from excited surface plasmons [28]; (3) energy damping [29]; (4) diffraction for high modes is not considered in Eq. (2) [14]. The intersections of k_{SSPP} and k_x-lines give the mode solutions. Point A ($f_{res} = 1.25$ THz) correspond to the fundamental mode for d = 48 μm, points B ($f_{res} = 0.67$ THz) and C ($f_{res} = 2.05$ THz) – the fundamental and 1st order modes for d = 94 μm. This values are in a very good agreement with resonance frequencies obtained in the reflection spectra (Figs. 5-6). The small deviation for the high order mode ($f_{res} = 2.05$ THz compared with 2.066 THz in the reflection spectrum) can be explained by the same reasons mentioned above [14].

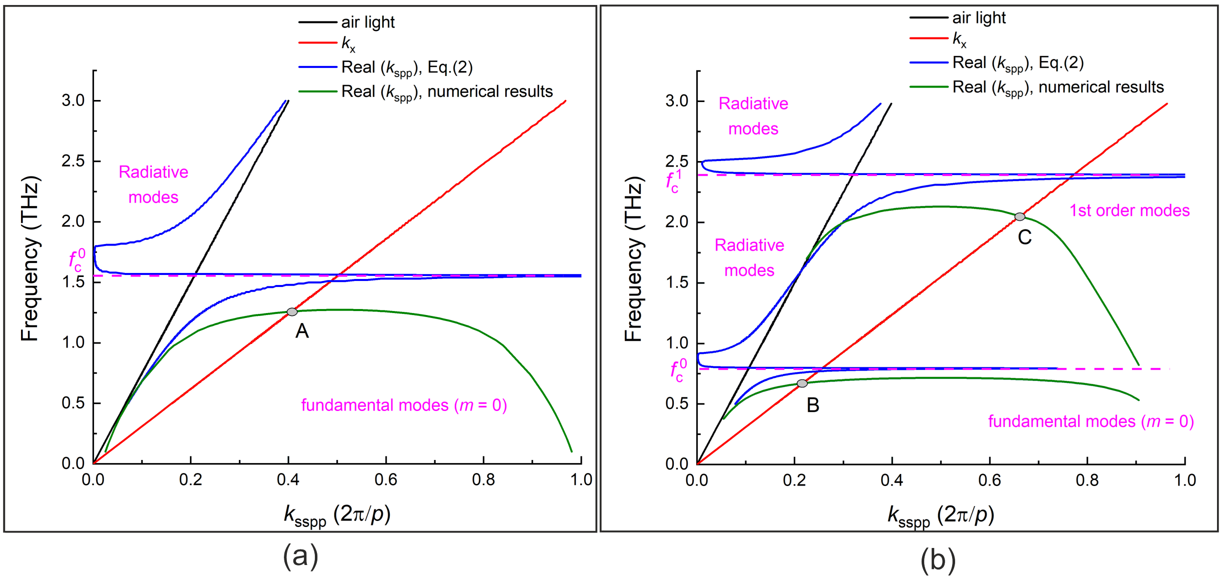

FIGURE 8. Dispersion curves for SSPPs on the gold rectangular gratings with p = 40 µm, w = 20 µm, d = 48 µm (a) and d = 94 µm (b). "Gas detector" ($n_g = n_d = 1$), $\theta_{int} = 45°$, n_p = 3.42. Black line – light in air, red line - projection of k_p-vector of the incident wave in the prism on to x-axis, blue line – real part of k_{SSPP} calculated from Eq.2, green line - k_{SSPP} vector obtained using Comsol software. The intersections of red and green lines give the mode solutions: point A ($f_{res} = 1.25\,\text{THz}$) – the fundamental mode for d = 48 µm; points B ($f_{res} = 0.67\,\text{THz}$) and C ($f_{res} = 2.05\,\text{THz}$) – fundamental and 1st order modes for d = 94 µm. f_c^0, f_c^1 - cutoff frequencies of fundamental and 1st order modes according Eq. (4).

CONCLUSIONS

In conclusion, we have numerically studied the sensing performance of a linear one-dimensional gold subwavelength rectangular grating platform with the ATR (Otto) coupling technique for gas detection in the THz range. The optimal parameters of gratings (the groove depth and gap between the prism and the grating) for exciting stable to the gap plasmon resonances with maximal efficiency were found. The dispersion analysis of surface waves on the gratings based on the effective medium model and Comsol simulations confirmed the correctness of the reflection spectrum simulations. The fundamental and 1st order modes of deep grooves demonstrated a very high sensitivity to a small refractive index change up to 1.5 THz/RIU (in the frequency domain) and 557 deg/RIU (in the angular domain), with the refractive index detection limit of the sensors $7\cdot10^{-3}$ RIU and $1.5\cdot10^{-7}$ RIU, respectively. Compared with the fundamental modes, the high-order modes revealed the higher *FOM* values up to 500 1/RIU due to the narrow width of the resonances. These sensing characteristics were comparable or exceeded the best results obtained with the similar sensing THz platforms.

ACKNOWLEDGMENTS

This work was done using the infrastructure of the Shared Research Facility "Siberian Synchrotron and Terahertz Radiation Centre" of BINP SB RAS and founded by Russian Foundation for Basic Research, grant number 16-32-00678.

REFERENCES

1. Joo-Hiuk Son, *Terahertz biomedical science&technology* (CRC Press, Boca Reton, 2014, pp. 117-266.

2. D.K. George, A.G. Markelz, “Terahertz Spectroscopy of Liquids and Biomolecules”, in *Terahertz Spectroscopy and Imaging*, edited by K E. Peiponen, A. Zeitler, M. Kuwata-Gonokami (Springer Series in Optical Sciences, vol 171. Springer, Berlin, Heidelberg, 2012), pp. 229-250.
3. R. Bogue, Sensor Review **38** (2), 216-222 (2018).
4. M. Naftaly, N. Vieweg, A. Deninger, Sensors (Basel) **19** (19), 4203 (2019).
5. Prabowo BA, Purwidyantri A, Liu KC. Surface Plasmon Resonance Optical Sensor: A Review on Light Source Technology. Biosensors (Basel). 2018;8(3):80.
6. T.-I. Jeon and D. Grischkowsky, “THz Zenneck surface wave THz surface plasmon propagation on a metal sheet,” Appl. Phys. Lett. 88, 061113 (2006).
7. J. B. Pendry, L. Martin-Moreno, and F. J. Garcia-Vidal, “Mimicking surface plasmons with structured surfaces” Science 305, 847–848 (2004)
8. F J Garcia-Vidal, L Mart´ın-Moreno, and J B Pendry. Surfaces with holes in them: new plasmonic metamaterials. Journal of Optics A: Pure and Applied Optics, 7(2):S97–S101, 2005.
9. Binghao Ng, Jianfeng Wu, Stephen M. Hanham, Antonio I. Fernández-Domínguez, Norbert Klein, Yun Fook Liew, Mark B. H. Breese, Minghui Hong, and Stefan A. Maier, Spoof Plasmon Surfaces: A Novel Platform for THz Sensing // Adv. Optical Mater. 2013, 1, 543–548
10. Zhijie Ma, Stephen M. Hanham, Paloma Arroyo Huidobro, Yandong Gong, Minghui Hong, Norbert Klein, and Stefan A. Maier, Terahertz particle-in-liquid sensing with spoof surface plasmon polariton waveguides // APL Photonics 2, 116102 (2017)
11. Xiaoyong Liu, Yijun Feng, Bo Zhu, Junming Zhao, and Tian Jiang, High-order modes of spoof surface plasmonic wave transmission on thin metal film structure // Optics Express, Vol. 21, No. 23, 31157 (2013).
12. Yusheng Zhang, Zhi Hong, Zhanghua Han, Spoof plasmon resonance with 1D periodic grooves for terahertz refractive index sensing // Optics Communications, 340, (2015), 102–106
13. Yi Huang, Shuncong Zhong, Tingting Shi, Yfo-Chun, Shen, Daziang Cui, Trapping waves with tunable prism-coupling terahertz metasurfaces absorber // Optics Express, Vol. 27, No. 18, 2019, 25647
14. Haizi Yao and Shuncong Zhong, High-mode spoof SPP of periodic metal grooves for ultra-sensitive terahertz sensing // Optics Express, Vol. 22, Issue 21, pp. 25149-25160 (2014)
15. Li Chen, Henghui Yin, Lin Chen & Yiming Zhu, Ultra-sensitive fluid fill height sensing based on spoof surface plasmon polaritons // Journal of Electromagnetic Waves and Applications, V. 32, 2018 - Issue 4.
16. Asmar Sathukarn, Chia Jia yi, Sakoolkan Boonruang, Mati Horprathum, Khwanchai Tantiwanichapan, Kiattiwut Prasertsuk, Chayut Thanapirom, Woraprach Kusolthossakul, and Kittipong Kasamsook, The Simulation of a Surface Plasmon Resonance Metallic Grating for Maximizing THz Sensitivity in Refractive Index Sensor Application // International Journal of Optics, V. 2020, Article ID 3138725, 8 pages
17. Borwen You, Ja-Yu Lu, Tze-An Liu, Jin-Long Peng, Hybrid terahertz plasmonic waveguide for sensing applications // Optic Express, Vol. 21, No. 18, 21087 (2013).
18. M. Born, E. Wolf, Principles of Optics (University Press, Cambridge, 1999)
19. A. Rusina, M. Durach, M. I. Stockman , Theory of spoof plasmons in real metals, Applied Physics A. 100 (2010) 375–378.
20. T. Jiang, L. Shen, X. Zhang, and L.-X. Ran, "High-order modes of spoof surface plasmon polaritons on periodically corrugated metal surfaces," Progress In Electromagnetics Research M 8, 91-102 (2009).
21. Kulipanov, G.N., Bagryanskaya, E.G., Chesnokov, E.N., Choporova, Y.Y., Getmanov, Y.V., Knyazev, B.A., Kubarev, V.V., Peltek, S.E., Popik, V.M., Salikova, T.V., Scheglov, M.A., Seredniakov, S.S., Shevchenko, O.A., Skrinsky, A.N., Veber, S.L., Vinokurov, N.A.: Novosibirsk free electron laser: facility description and recent experiments. IEEE Trans. Terahertz Sci. Technol 5, 798 (2015)
22. Antsygin, V. D.; Mamrashev, A. A.; Nikolaev, N. A.; Potaturkin, O. I.; Bekker, T. B.; Solntsev, V. P. Optical properties of borate crystals in terahertz region. Opt. Commun. 2013, 309, 333–337.
23. B.G. Goldenberg, A.G. Lemzyakov, V.P. Nazmov, V.F. Pindyurin, A.G. Zelinsky, Multibeam X-ray lithography to form deep regular microstructures, Journal of Surface Investigation: X-Ray, Synchrotron and Neutron Techniques. 10 (2016) 92–95.
24. Ghoneim, Mohamed; Hussain, Muhammad (1 February 2017). "Highly Manufacturable Deep (Sub-Millimeter) Etching Enabled High Aspect Ratio Complex Geometry Lego-Like Silicon Electronics" (PDF). *Small*. **13** (16): 1601801.
25. M. Ordal, L. Long, R. Bell, S. Bell, R. Bell, R. Alexander Jr, and C. Ward, "Optical properties of the metals al, co, cu, au, fe, pb, ni, pd, pt, ag, ti, and w in the infrared and far infrared," Appl. Opt. 22(7), 1099-1119 (1983).

26. J. Homola, S.S. Yee, G. Gauglitz, Surface Plasmon resonance sensors: review, Sens. ActuatorsB—Chem. 54 (1999) 3–15.
27. K. Johansen, H. Arwin, I. Lundström, and B. Liedberg, "Imaging surface plasmon resonance sensor based on multiple wavelengths: Sensitivity considerations," Rev. Sci. Instrum. 71(9), 3530-3538 (2000)
28. H. Hirori, M. Nagai, and K. Tanaka, "Destructive interference effect on surface plasmon resonance in terahertz attenuated total reflection," Opt. Express **13**(26), 10801-10814 (2005)
29. A. Otto, "Excitation of nonradiative surface plasma waves in silver by the method of frustrated total reflection," Z. Angew. Phys. **216**(4), 398-410 (1968)